

Article

# Spatiotemporal Variations of Precipitation in the Southern Part of the Heihe River Basin (China), 1984–2014

Xuezhen Zhang <sup>1,2,\*</sup>, Pei Li <sup>3</sup> and Deshuai Li <sup>4</sup>

<sup>1</sup> Key Laboratory of Land Surface Pattern and Simulation, Institute of Geographical Sciences and Natural Resources Research, Chinese Academy of Sciences, Beijing 100101, China

<sup>2</sup> College of Resources and Environment, University of the Chinese Academy of Sciences, Beijing 100049, China

<sup>3</sup> Unit 95810 of PLA, Beijing 100010, China; lpatmos@163.com

<sup>4</sup> Unit 93995 of PLA, Xi'an 710300, Shanxi, China; lidsh06@163.com

\* Correspondence: xzzhang@igsnr.ac.cn

Received: 22 December 2017; Accepted: 27 March 2018; Published: 1 April 2018



**Abstract:** Local precipitation variations in the context of global warming are a hot topic in the climate change research community. Using daily precipitation data spanning from 1984 to 2014 from 25 meteorological stations, the spatiotemporal variations of precipitation were analyzed for the southern part of Heihe River Basin (HRB), which is the second-largest inland river basin in Northwest China. Linear trend analysis, empirical orthogonal function (EOF) analysis, the Mann–Kendall test, and the moving *t*-test were employed in the study. Results showed that the regional annual precipitation exhibited an increasing trend with a slope of 13.1 mm per decade from 1984 to 2014. The increasing trend was detected at 21 sites and the first EOF illustrating the regional increasing trend explained 51.8% of the total variance. The increasing trend of annual precipitation was mainly due to an increase in autumn precipitation, while summer precipitation exhibited a weak declining trend and spring–winter precipitation remained unchanged. Moreover, the increasing precipitation trend was mainly caused by an abrupt increase around 1997, when the global warming hiatus occurred. Through 1997, the atmospheric circulation and physical structure, such as vertical upward motion, vapor transmission, and its convergence changed to be more favorable for precipitation in autumn, but unfavorable for precipitation in summer in the HRB.

**Keywords:** precipitation; spatiotemporal variations; global warming; atmospheric circulation; the Heihe River Basin; Northwest China

## 1. Introduction

As the only source of water in the inland watershed of an arid area, precipitation not only determines the categories and spatial distribution of natural ecosystem, but also plays a crucial role in agricultural yield, economic development, and societal statues [1,2]. Therefore, studies on inland watersheds of arid areas are very valuable [2,3]. The Heihe River, which is located in arid and semi-arid regions of Northwest China, is the second-largest inland river of China, with a length of 821 km and drainage area of 130,000 km<sup>2</sup>. Geographic conditions exhibit large spatial differences within the Heihe River Basin (HRB). From south to north, there are three major geomorphological sub-regions. In the southern part, there is the Qilian Mountains, with remarkable vertical zonality. It is the water source of HRB and the elevation of the area ranges from 2000 m to 5500 m. In the middle, there is Hexi Corridor, where the elevation decreases from 2000 m to 1000 m. It is located between the Qilian Mountains and the Beishan Mountains. In the northern part, there is the Alxa high-plain. It is mainly occupied by bare

Gobi, with a mean altitude of about 1000 m. The seasonal distribution of precipitation within one year was characterized by the maximum in summer, followed by spring and autumn, and minimum in winter [4,5]. The economy, agriculture, and human living conditions in the HRB are highly dependent on the streamflow of the Heihe River [4–6]. The shortage of water resources is the most pressing issue for the survival and development of the HRB [7]. Hence, the precipitation variations in the HRB have been the subject of many studies [4–9].

Previous studies have focused on the temporal and spatial variations of the precipitation and the factors determining precipitation in the HRB. For instance, Ding et al. [4] reported that from 1959 to 1999 precipitation tended to increase across the entire HRB, but with differences between alpine and plains areas. It was also found that 1959–1999 was divided into two stages at 1980. Before that there was a strong increasing trend and thereafter precipitation tended to decrease markedly. Based on 10 meteorological stations within the HRB, Wang and Niu [9] reported that precipitation exhibited a slightly increasing trend in the upstream mountain area and a decreasing trend for both the agricultural area in the middle reach and the desert area in the lower reach since 1950. By synthesizing the existing achievements, it was found that on the whole the annual average values of precipitation, which increased slightly during the last several decades, were still between 50 and 500 mm, and the distribution of precipitation was very uneven spatially, with more in the southeast and less in the northwest [7–12]. However, almost all of these studies are based on station data from the last century, and most of them on no more than 10 sites. Due to the shortage of observed data in West China, the knowledge on the spatiotemporal variations of precipitation in the HRB may be limited. Additionally, to date, there are few studies investigating the changes in atmospheric circulations leading to precipitation in the HRB.

From the late 1990s to the early 2010s, global mean surface temperature has increased more slowly than in the preceding two decades [13]. In the wake of the release of the Working Group I contribution to the 5th Assessment Report of the Intergovernmental Panel on Climate Change (IPCC AR5), there has been much attention in the media and scientific community devoted to the so-called hiatus [14,15]. In the context of global warming and its hiatus, the regional temperature of HRB exhibited strong warming from the 1960s to the 1990s and very weak warming, which is like the hiatus, from the late 1990s to the early 2010s [16]. There have been many studies on local/regional precipitation variations as a response to climate warming. So far, the responses of regional/local climate within China to climate warming and its hiatus have been little studied. In this study, the spatial and temporal variations of precipitation over the HRB were examined using observational precipitation data from 25 meteorological stations from 1984 to 2014. In addition, the changes in atmospheric circulation leading to precipitation from 1984 to 2014 were investigated to understand the cause of precipitation changes. These results are expected to improve our understanding of the regional climate changes of HRB, especially in the context of the global warming hiatus.

## 2. Data and Methodology

### 2.1. Data

This study used rain gauge measurements of precipitation from meteorological stations. Following the stipulation that daily measurements from January 1984 to December 2014 had to be exactly consecutive without missing values, 25 meteorological stations within the HRB were selected (see Table 1 for details). Figure 1 shows that all stations were located in the southern part of the HRB, referring to the upper and middle reaches of the Heihe River. Such uneven distribution is mainly derived from the spatial variability of precipitation. Within the HRB, precipitation mostly occurs in the upper and middle reaches and there is very little precipitation in the lower reach [7,11]. As a result, there are plenty of water resources and a high population in the upper and middle reaches, and less water and a lower population in the lower reach. Additionally, due to the complex terrain of the upper reach, there is a higher population in the middle reach than in the upper reach. So, as we can see, there are many meteorological stations in Hexi Corridor along the foothills of the Qilian Mountains.

Meanwhile, the measurements from these meteorological stations generally represent the regional precipitation of HRB, since the precipitation mostly occurs in the upper and middle reaches.

**Table 1.** Meteorological stations used in this study.

Number	Station	Longitude/ $^{\circ}$ E	Latitude/ $^{\circ}$ N	Altitude/m
1	Zhashimake	100.12	38.21	2645
2	Qilian	100.24	38.19	2657
3	Yingluoxia	100.18	38.81	1623
4	Maying	101.19	38.34	2466
5	Liqiao	101.13	38.51	2134
6	Dahuangshan	101.22	38.45	2434
7	Xiakou	101.42	38.51	2229
8	Biandukou	100.94	38.24	2752
9	Binggoutai	100.84	38.29	2684
10	Shuangshusi	100.83	38.35	2467
11	Liuba	100.74	38.63	1826
12	Wafangcheng	100.5	38.47	2345
13	Gaoya	100.36	38.61	1362
14	Kangle	99.92	38.8	2585
15	Sunan	99.63	38.84	2212
16	Pingchuan	100.11	39.31	1335
17	Dahe	99.51	39	2609
18	Hongshahe	99.2	39.18	2249
19	Fenglehe	98.82	39.35	1986
20	Zhengyixia	99.46	39.82	1219
21	Hongsihu	101.2	39	1730
22	Zhulongguan	97.98	39.18	2842
23	Xindi	98.42	39.56	1812
24	Hongshan	98.65	39.44	1830
25	Yuanyangchi	98.83	39.91	1317

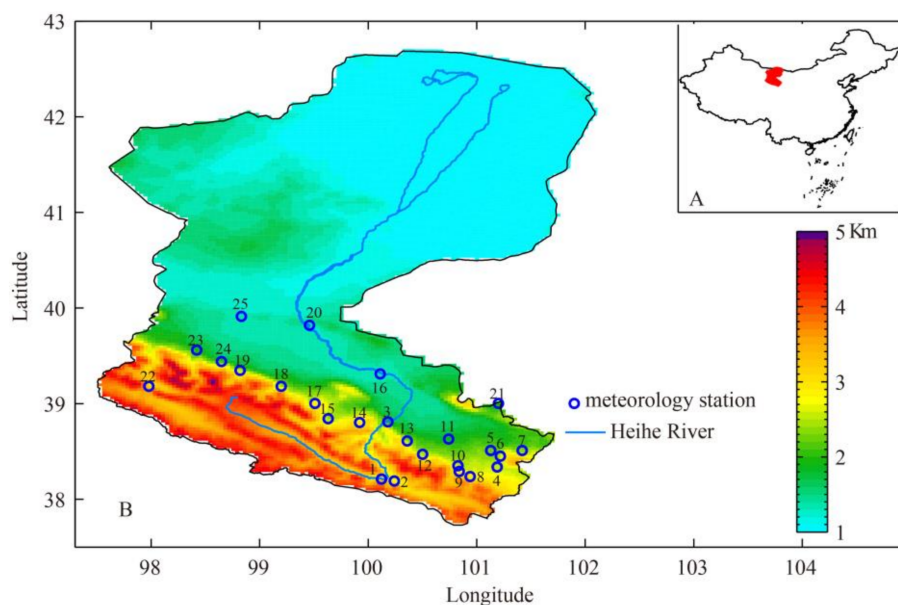


**Figure 1.** Location and terrains of the study area. (A) Location of the HRB in China; (B) the terrain of the HRB (the colored patches denote the elevation above sea level) and the 25 meteorological stations used in this study (see Table 1 for details).

This study also used the reanalysis data from the European Centre for Medium-Range Weather Forecasts (ECMWF) Interim from 1984 to 2014. The monthly mean geopotential height, temperature,

wind, vertical velocity, water vapor flux, and its divergence fields from the ECMWF Interim were analyzed. The ECMWF Interim reanalysis data has a spatial resolution of  $1^\circ$  (latitude)  $\times$   $1^\circ$  (longitude).

## 2.2. Methodology

This study disclosed the spatiotemporal characters of precipitation variations in the southern part of the HRB from 1984 to 2014, and analyzed the potential physical mechanisms leading to the precipitation changes. The spatiotemporal character of the precipitation variations were disclosed through three aspects: (1) linear trend of precipitation and its spatial variability; (2) dominant spatiotemporal modes of precipitation variations; and (3) abrupt change of precipitation.

Firstly, with the least squares method, the linear trend of precipitation was fitted. This study disclosed the linear trend of precipitation amount and number of days with precipitation (NDP), respectively, for each station and for the mean of the 25 stations from 1984 to 2014. Here, the precipitation amount refers to the sum of daily precipitation within a certain period, such as annually, seasonally, or monthly. A day with precipitation was defined as daily precipitation greater than 0.1 mm.

Second, to extract the dominant spatiotemporal modes of precipitation variations, we conducted an empirical orthogonal function (EOF) analysis. EOF analysis is actually principal component analysis (PCA), which operates on the spatial–temporal matrix [17]. One station is treated as one variable and one time point is treated as one observation. In detail, before the EOF analysis, the annual precipitation series from 1984 to 2014 were normalized for each station.

The normalized precipitation series from the 25 stations were grouped into a matrix  $P_{M \times N}$  where  $M$  and  $N$  denote the station numbers and total years, respectively. Using Equation (1), the correlation coefficient matrix  $R_{M \times M}$  was built. In the matrix  $R$ , the component  $r_{ij}$  records the correlation coefficient of annual precipitation between site  $i$  and site  $j$ . Next, with the Jacobian method, the eigenvalue  $V\{v_1, v_2, \dots, v_M\}$  and eigenvectors  $E\{e_1, e_2, \dots, e_M\}$  of the matrix  $R$  were calculated. The  $v_i$  and  $E_{i(M \times 1)}$  denote the  $i$ -th eigenvalue and eigenvector, respectively. Next, using Equation (2), the time coefficient, namely  $PC$ , was calculated. Following the structure of  $P_{M \times N}$ , in which spatial samples are row vectors, the components of  $e_i$  corresponded to stations one by one. So, the  $e_i$  could be expressed as a map that illustrates the spatial pattern of precipitation variations, namely  $EOF$ . The  $PC$  illustrates the temporal characters of  $EOF$ . Generally, the first several  $EOF$ s contain mostly variations of precipitation. The variation of each  $EOF$  could be quantified by the weighting coefficient, which was calculated by Equation (3). Therefore, only the first several  $EOF$  and  $PC$  were analyzed in practice.

$$R_{M \times M} = P \times P^T / (N - 1) \quad (1)$$

$$PC = P^T \times E, \quad (2)$$

where  $P_{M \times N}$  denotes the precipitation from  $M$  stations and  $N$  years;  $P^T$  denotes the transposition of  $P_{M \times N}$  and  $E$  denotes the eigenvectors matrix.

$$Wi = v_i / (v_1 + v_2 + \dots + v_M), \quad (3)$$

where  $v_i$  denotes the  $i$ -th eigenvalue.

Third, to detect the abrupt changes of annual precipitation from 1984 to 2014, the Mann–Kendall (M–K) test and moving  $t$ -test were conducted. The sequential M–K test, as a non-parametric test, is widely used to detect the monotonic trend in a series of environmental data, climate data, and hydrological data [18–20]. In detail, following Equation (4), an order serial  $S_k$  was built using the original precipitation series. Then, following Equation (5), the serial  $UF_k$  was built using the order serial  $S_k$ . These definitions implicated that  $UF_k$  represented the trend of temporal serial from begin to the time  $k$ . Next, we reversed the order of the  $P_i$  series and calculated Equations (4) and (5) again. There would be a new  $UF_k$  serial. Here, we defined  $UB_k = -1 \times UF_k$  and  $k = n - k + 1$ . The  $UB_k$  represents the reverse trend of series from end to the time  $n - k + 1$ . As a result, the intersection points

of  $UF_k$  and  $UB_k$  denote the reverse trend to the original precipitation series, and were hence treated as abrupt change points.

$$S_k = \sum_{i=1}^k \sum_{j=1}^{i-1} a_{ij} (k = 2, 3, 4, \dots, n), \quad (4)$$

where  $a_{ij} = \begin{pmatrix} 1, & P_i > P_j \\ 0, & P_i < P_j \end{pmatrix}$ ,  $P_i$  is the precipitation in  $i$  year.

$$UF_k = \frac{[S_k - E(S_k)]}{\sqrt{Var(S_k)}} (k = 1, 2, \dots, n), \quad (5)$$

where  $E(S_k) = k(k+1)/4$ ;  $Var(S_k) = k(k-1)(2k+5)/72$ .

The moving  $t$ -test is actually the Student's  $t$ -test on two consecutive windows of precipitation series. By building  $t$ -statistic model, the significance of the differences of the mean values of two consecutive windows was tested. In this study, the window size was defined as five years and a confidence level of 0.05 was applied. Once the differences of the mean values of two consecutive windows were significant, abrupt change was considered to be occurring. Though the methodologies of the moving  $t$ -test and M-K test were different, the abrupt changes detected with the two methods may be comparable with each other, as the large trend reverse of  $UF$  and  $UB$  series generally co-occurs with a large change in mean values.

Final, to understand the physical mechanisms leading to the precipitation changes, the changes of atmospheric circulation corresponding to the precipitation changes was investigated. According to the results of the M-K test and moving  $t$ -test, the study period of 1984–2014 was divided into two periods, 1984–1997 and 1998–2014. The differences of average geopotential height, temperature, and wind at a pressure level of 500 hPa between the two periods were analyzed. These differences represented the atmospheric circulation changes. In addition, we analyzed the differences of average temperature and vertical velocity on the vertical cross section, the column integrated water vapor flux, and its divergence between the two periods.

### 3. Results

#### 3.1. Spatial and Temporal Patterns of Precipitation Variations in the HRB

Figure 2 shows that both the annual mean precipitation amount and NDP exhibited a general declining trend from southeast to northwest. The mean annual precipitation amount and NDP of the 25 stations for the 1984–2014 were 259.6 mm and 72.4 days, respectively. Among the station-based measurements, the annual precipitation reached as high as 532.9 mm at Maying Station in the southeast but was only 62.8 mm at Yuanyangchi Station in the northwest. Correspondingly, the annual NDP was as high as 101.2 days at Maying Station and was only 32.5 days at Yuanyangchi Station.

Due to a lack of ground stations in the Qilian Mountains, the general spatial variability in the mountain areas was derived from spatial interpolation (Figure 2). However, the spatial variability derived from interpolation and that derived from dynamics-based climate modeling could be comparable with each other. For instance, the several years of high-resolution (3–5 km) simulations with Weather Research and Forecast (WRF) model also show that the western part of the Qilian Mountain has less precipitation than the southeastern part [21,22] It is noted that simulated precipitation is significantly larger than the station measurements in the mountainous area due to the high sensitivity of the micro-physical parameters of the WRF model to complex terrain [22].

The precipitation of HRB also exhibit seasonal cycles (Figure 3). There is more precipitation and NDP in summer with a maximum in July and less precipitation and NDP in winter with the minimum in January. In the summer, the monthly mean precipitation amount and NDP of 25 stations for 1984–2014 were in the ranges of 45–55 mm and 14–18 days, respectively. In the spring and autumn, they are 5–35 mm and 5–12 days, respectively. In the winter, they are only around 5 mm and five days.

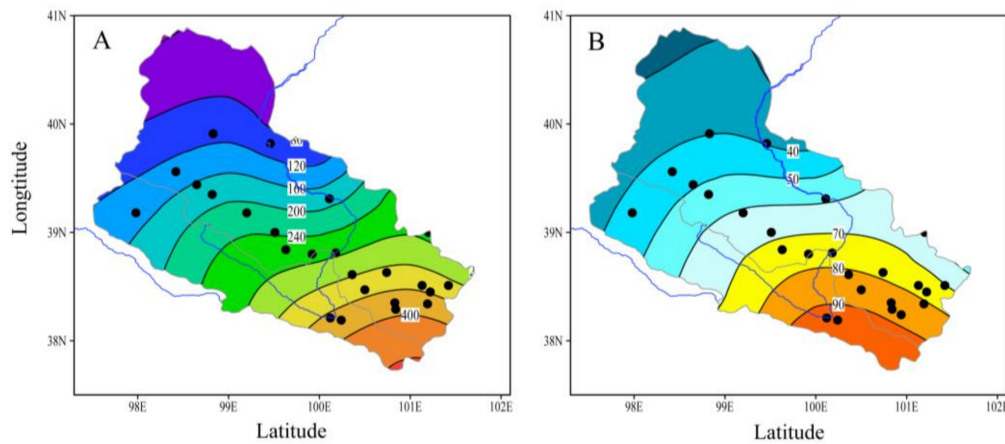


**Figure 2.** Spatial distribution of total annual precipitation amount ((A); unit: mm) and number of days with precipitation (NDP) ((B); unit: day) in the HRB from 1984 to 2014 (black dots represent meteorological stations).

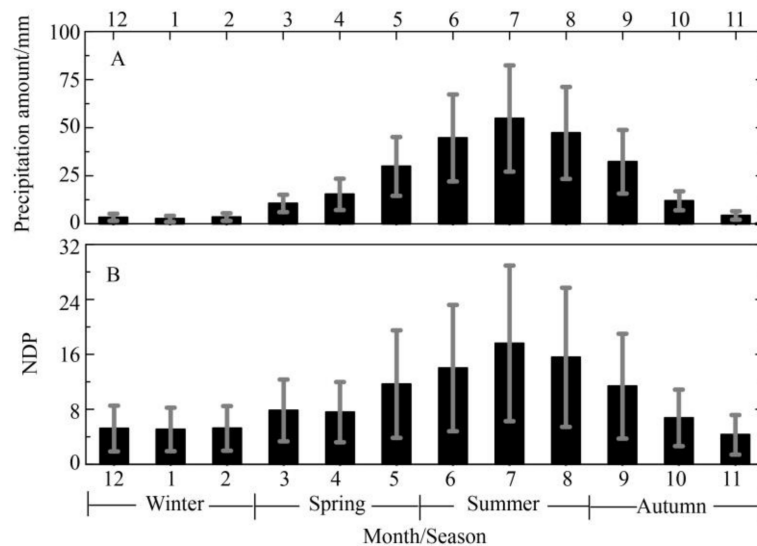


**Figure 3.** Monthly mean precipitation amount (A) and number of days with precipitation (NDP; (B)) of 25 stations in HRB for 1984–2014 (error bar denotes maximum to minimum of 25 stations).

From 1984 to 2014, there were extensively increasing trend for the annual precipitation amount and NDP in the southern part of HRB (Figure 4A,C). Among the 25 stations, the number of stations with increased precipitation and NDP were 19 and 21, respectively. The linearly increasing trends passed statistical significance (at the  $p < 0.1$  level) from six and 10 stations for precipitation amount and NDP, respectively. As a result, the mean annual precipitation and NDP of all 25 stations increased by 13.1 mm and 3.2 days per decade, respectively, from 1984 to 2014.

The variations of precipitation from 1984 to 2014 exhibited large differences between seasons. The mean precipitation of 25 stations in spring and winter exhibited a very weak linear trend, with a slope of 2.6 and 1.8 mm per decade, respectively, from 1984 to 2014 (Figure 5). The precipitation in summer showed a slight downward trend, but a significant increasing trend in autumn. The precipitation amount and NDP increased by about 14.4 mm and 3.9 days per decade from 1984 to 2014 in autumn (Table 2), respectively. It can be concluded that the increase in annual precipitation, as shown by Figure 4, was mainly due to the increase in autumn precipitation.

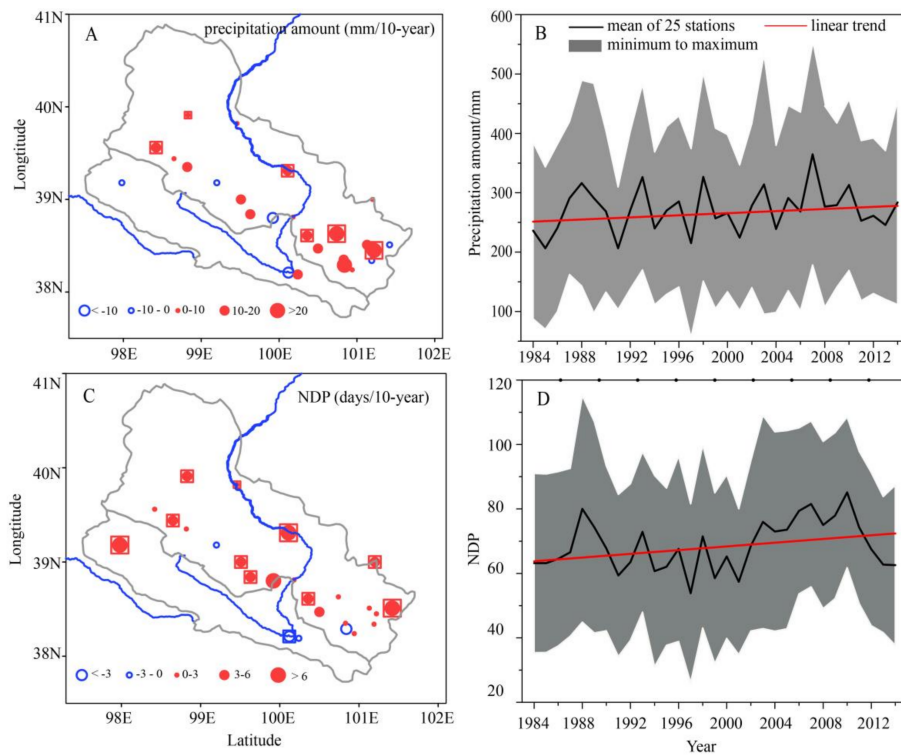


**Figure 4.** The linear trend of annual precipitation amount (A,B) and number of days with precipitation (NDP; C,D) for the 25 stations from 1984 to 2014. In (A) and (C), the dots inside squares denote significance at a level of 0.1.

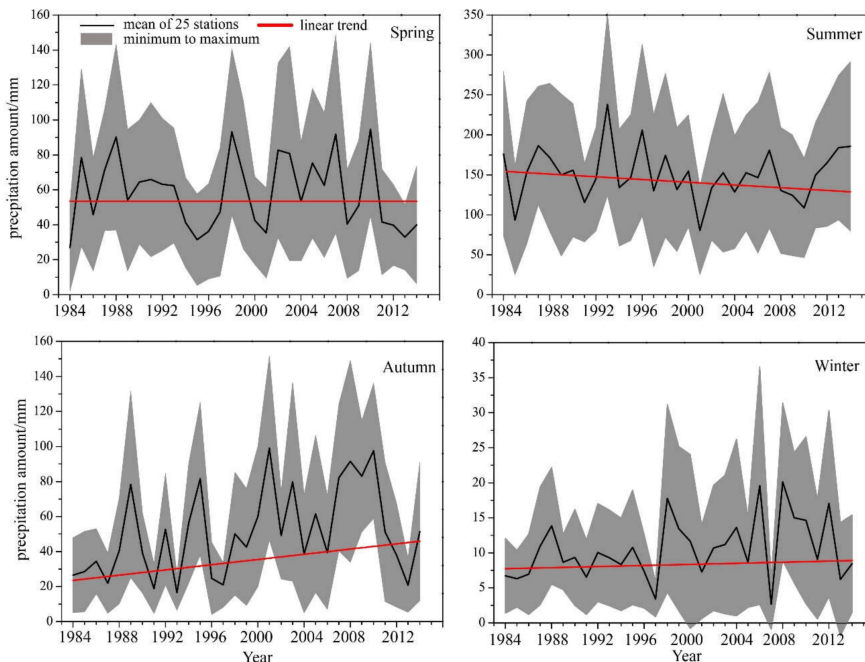


**Figure 5.** The mean precipitation amount variations of 25 stations in HRB for the spring (March to May), summer (June to August), autumn (September to November), and winter (December to February), respectively, from 1984 to 2014.

**Table 2.** The linear trend of precipitation amount and number of days with precipitation (NDP) for each season from 1984 to 2014.

	Annual	Spring	Summer	Autumn	Winter
Precipitation amount (mm/10-year)	13.1	2.6	−5.7	14.4	1.8
NDP (days/10-year)	3.2	−5.3	0.7	3.9	0.7

### 3.2. EOF Analysis of Precipitation in the HRB

The cumulative variance explained by the first two EOFs reached about 67.3% (Table 3). Hence, the first two EOFs explained most of the precipitation variation of 25 stations from 1984 to 2014. The first EOF explained 51.8% of the total variance of annual precipitation. Figure 6 show that this EOF exhibits uniform behavior across the study area. Such a spatial pattern suggests that precipitation changes would be in the same phase across the entire region. The corresponding PC exhibited high values in 2007, 2010, 1993, and 1998; and low values in 1997, 1985, 1991, and 2001. These high and low values suggest that there would be more and less precipitation across the entire region, respectively. Thereby, these high and low values explained the positive and negative anomaly of regional mean precipitation (Figure 4B), respectively. Additionally, PC1 exhibited a positive trend, which suggests a regional increase in annual precipitation. Hence, such a positive trend may also explain the increasing trend of regional mean precipitation (Figure 4B). The uniform behavior of EOF1 indicates that such spatial–temporal variation of precipitation may be induced by a large-scale weather system.

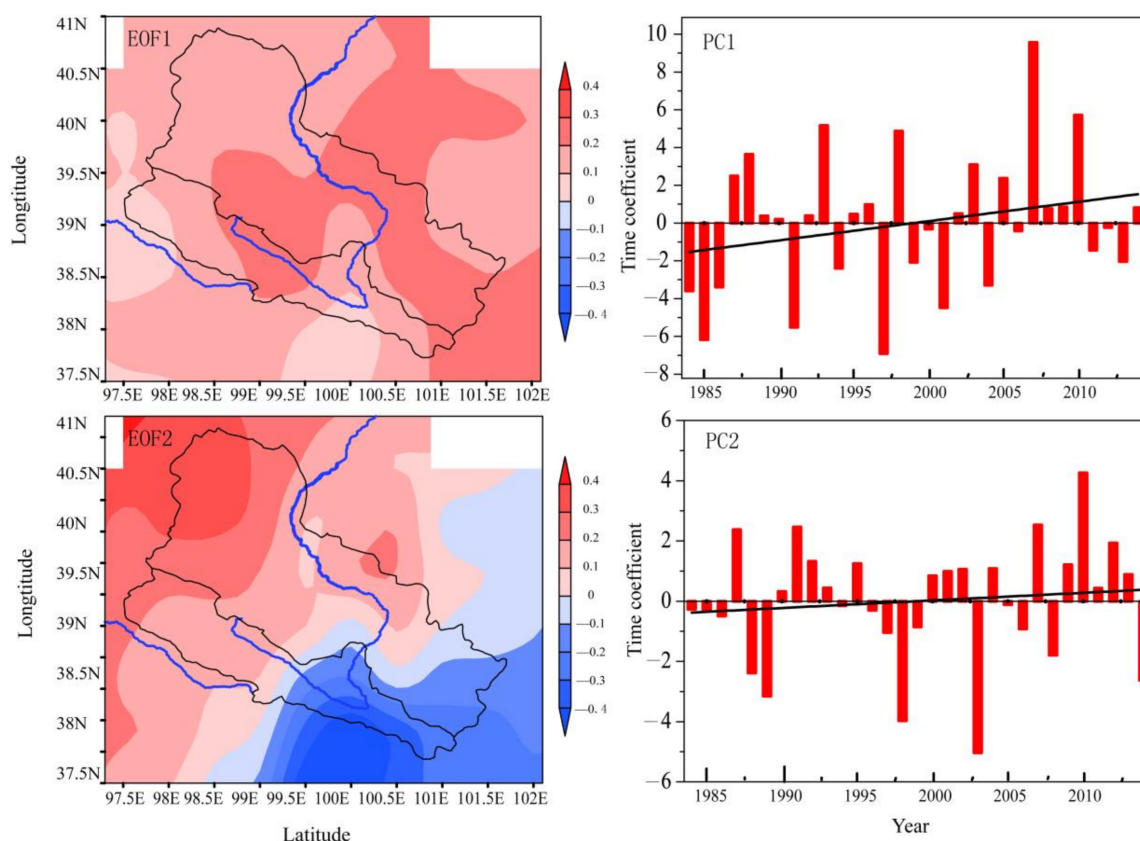


**Figure 6.** The first two EOFs (left) and its time coefficients, i.e., PCs (right) for annual precipitation variations from 25 stations in HRB from 1984 to 2014.

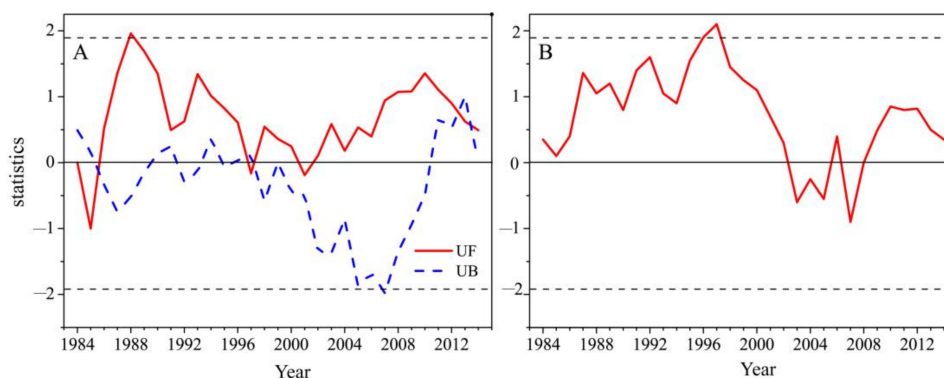
**Table 3.** Explained variance of the first two EOFs of the normalized precipitation amount from 25 stations in HRB from 1984 to 2014.

EOF	1	2
Explained variance (%)	51.8	15.5
Cumulative variance contribution (%)	51.8	67.3

The second EOF explained 15.5% of the total variance. This EOF exhibits an approximately dipole structure (Figure 6). There was a negative center in the southeast and a positive center in the northwest, respectively. Such a spatial pattern suggests that the precipitation variations in the southwest would be out of phase with those in the northwest. The corresponding PC2 exhibited the highest and lowest values in 2010 and 2003, respectively. It is suggested that there was much more precipitation in the southeast and less precipitation in the northwest in 2003 and the spatial distribution of precipitation anomaly is the reverse in 2010. This EOF may explain more precipitation, reaching up to 585.3 mm in the Zhashimake (No. 1) in 2003, accounting for 140.1% of climatology mean value, and less precipitation reaching as low as 41.6 mm in Yuanyangchi (No. 25) in 2003, accounting for only 65.3% of climatology mean value. Moreover, this EOF explained the precipitation being as low as 300.2 mm in Zhashimake (No. 1) and reaching up to 143.2 mm in Yuanyangchi (No. 25) in 2010. Additionally, PC2 exhibited a slight increasing trend, which may indicate increasing precipitation in the northwest and decreasing precipitation in the southeast from 1984 to 2014. Such a reverse trend suggests weakening precipitation differences between the southeast and northwest.

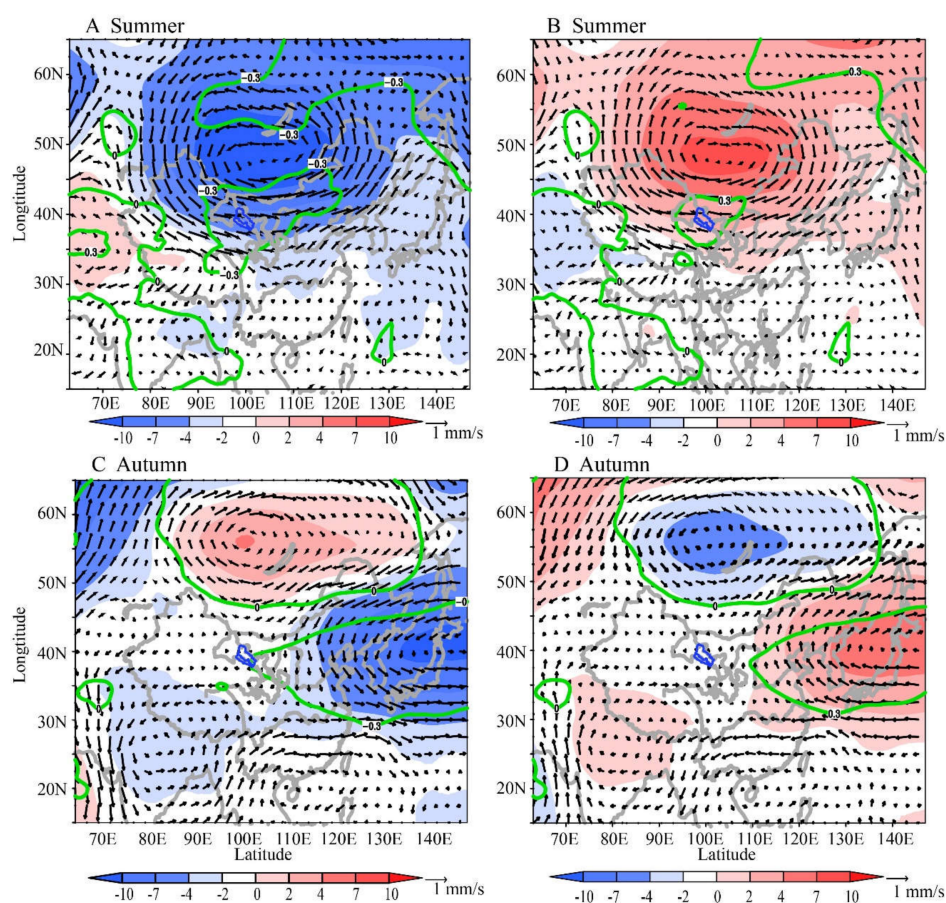
### 3.3. Abrupt Change of the Time Series

Figure 7A shows that the UF series mostly remained positive, without exceeding the significance level line. It is suggested that precipitation showed a slight increase in HRB from 1984 to 2014. There were two intersections between the UF and UB series in 1997 and 2012 (Figure 7A), respectively. The intersections suggest that the precipitation might have changed abruptly around 1997 and 2012. The moving  $t$ -test shows a significant breaking point in 1997 at a confidence level of 0.05 (Figure 7B). Such statistical detection indicates that there was a precipitation uplift around 1997. The mean precipitation was 252 mm in 1993–1997 and increased to 259 mm in 1998–2002. Thereby, the M–K test and moving  $t$ -test suggest that there was a sudden increase in precipitation around 1997. The mean precipitation was 251 mm in 1984–1997 and increased to 268 mm in 1998–2014. As shown in Figure 4, the abrupt increase was mainly caused by autumn precipitation, which increased from 37 mm in 1984–1997 to 58 mm in 1998–2014. The abrupt change corresponded to the beginning of the climate warming hiatus. The regional precipitation increased, especially in the autumn.

**Figure 7.** The time series from sequential Mann–Kendall statistics (A) and moving  $t$ -test (B) of mean annual precipitation of 25 stations from 1984–2014. UF and UB indicate the progressive and retrograde curve, respectively. Horizontal dashed lines denote the confidence at level of 0.05.

### 3.4. Differences in Circulation Characteristics

The abovementioned findings demonstrate that the precipitation in summer and autumn changed greatly. To understand the potential mechanisms leading to the precipitation changes, the changes of atmospheric circulation from 1984–1997 to 1998–2014 were analyzed for summer and autumn, respectively. Figure 8 shows that in summer time a geopotential height of 500 hPa in the middle and high latitudes exhibited a low-pressure anomaly in 1984–1997 (Figure 8A). However, there was a high-pressure anomaly over that area in 1998–2014 (Figure 8B). Due to conversion from low-pressure anomaly to high-pressure anomaly, the cyclonic circulation anomaly in 1984–1997 over that area was replaced by the anticyclonic circulation anomaly in 1998–2014. Furthermore, the atmospheric circulation situation also changed from convergence to weak divergence. Since divergence is unfavorable for precipitation, the changes in atmospheric circulation from convergence to weak divergence may have led to the declining precipitation trend from 1984 to 2014. For the autumn, the geopotential height of 500 hPa was characterized by high-pressure anomaly over Mongolia and low-pressure anomaly over the Sea of Japan in 1984–1997 (Figure 8C,D). Over the HRB, the upper air was dominated by anti-cyclone circulation and dry-cold northwest wind. Such circulation is unfavorable for precipitation. In 1998–2014, the anomaly of geopotential height of 500 hPa was completely different than that in 1984–1997. Over the HRB, there was a dominant moist southwest wind from the ocean or an anomaly cyclonic. Such circulation is favorable for precipitation. The abovementioned changes in circulations at a pressure level of 500 hPa explained the decrease in summer precipitation and increase in autumn precipitation from 1984 to 2014.



**Figure 8.** Anomaly of wind (arrows; unit: m/s), temperature (green contour line; unit: °C), and geopotential height (shading; unit: GPM) at a pressure level of 500 hPa in 1984–1997 (left) and 1998–2014 (right) for summer (top) and autumn (bottom), referring to the mean of 1984–2014.

Vertical movement and water vapor transmission are also necessary conditions to induce precipitation. Figure 9 shows the changes of vertical movement from 1984–1997 to 1998–2014. It can be seen that, within the range of 98E–102E, the airflow has an ascending motion between the 700 hPa and 400 hPa height layers in autumn. In the summer, airflow showed upward movement in the eastern region, while there was downward movement in the western region. This finding illustrates that, compared with 1984–1997, the vertical upward movement of airflow was significantly stronger in 1998–2014, especially in the autumn. However, the vertical profiles of temperature changes demonstrate that thermal conditions were likely unfavorable for vertical upward movement, since warming was gradually intensified from the bottom to the top of the atmosphere. Hence, the strengthened upward movement may be caused by large-scale changes in dynamic conditions, rather than changes in local thermal conditions.

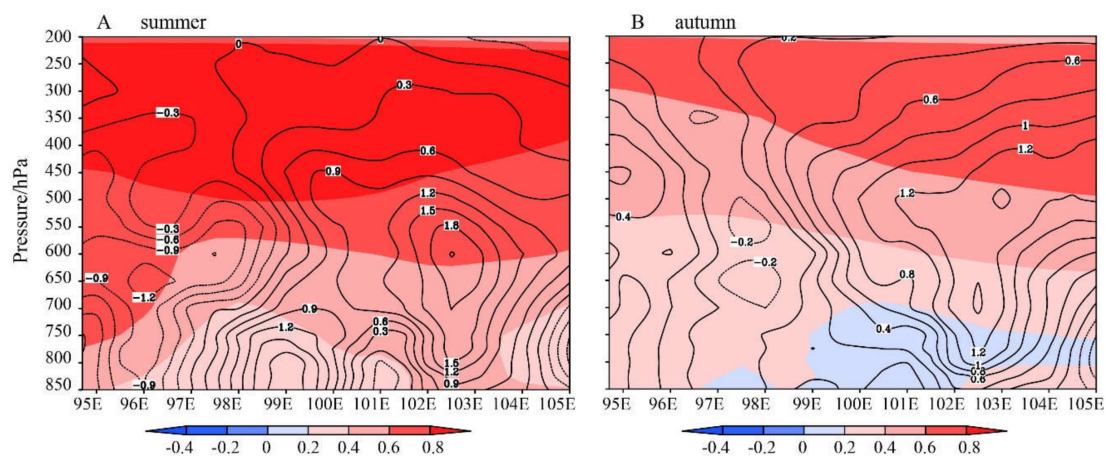
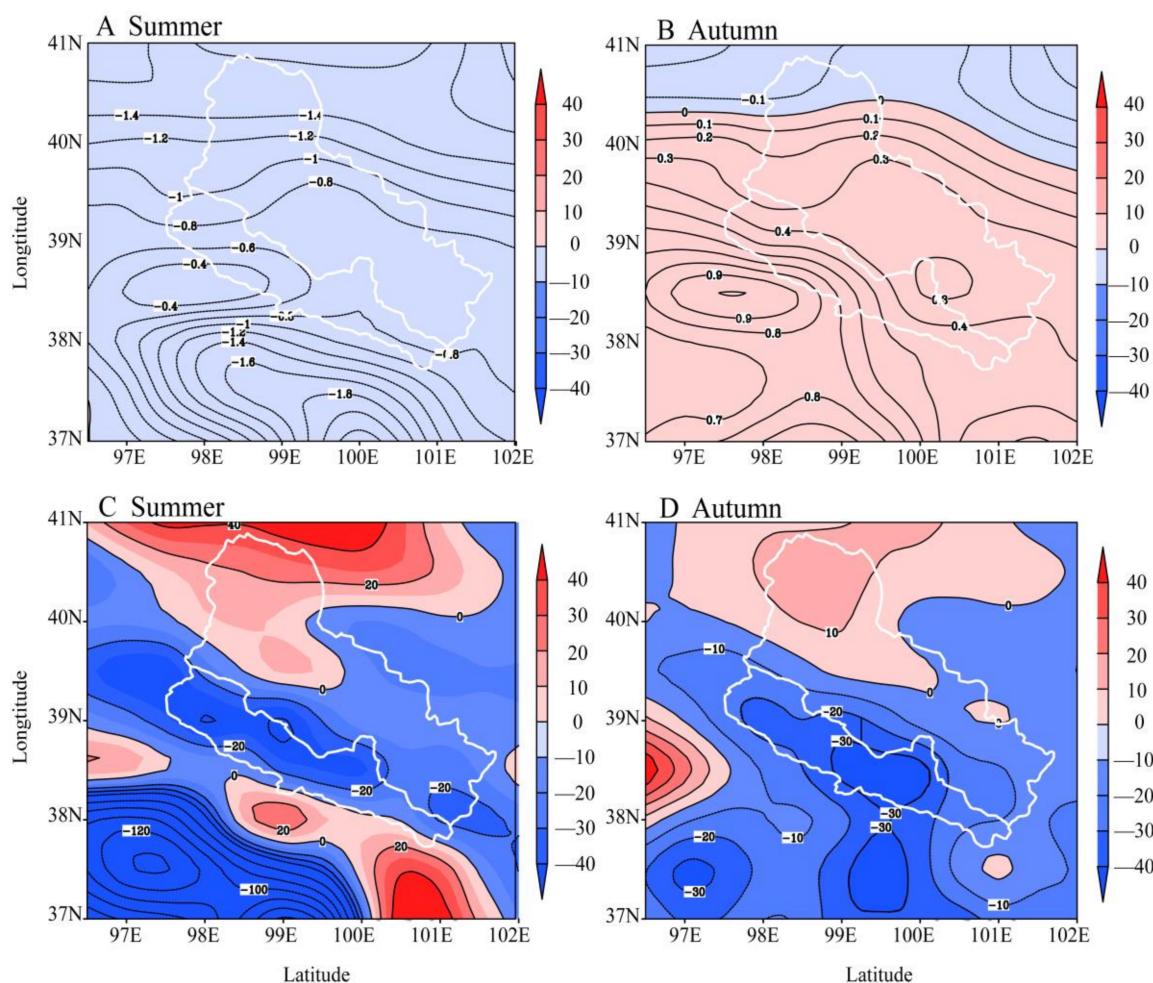


**Figure 9.** The differences in temperature (shading; unit: °C) and vertical velocity (contour line; unit:  $-0.01 \text{ Pa s}^{-1}$ ) for 1998–2014 subtract 1984–1997 on the vertical cross section of the HRB (38N–40N) for summer (A) and autumn (B).

Figure 10 shows that the difference in vertically integrated column water vapor flux through 1998–2014 subtracted 1984–1997 was positive in autumn, whereas it was negative in summer for the whole study area. This finding suggests that there was more water vapor in autumn in 1998–2014 than in 1984–1997. However, for the summer, the water vapor in 1998–2014 was less than that in 1984–1997. Meanwhile, the divergence of water vapor flux was negative, which suggests the convergence of water vapor. The convergence of water vapor is favorable for precipitation. These findings demonstrate that both the increase in water vapor flux and the dynamic conditions of convergence were favorable for precipitation in autumn from 1984 to 2014. For the summer, the dynamic condition of convergence was favorable for precipitation, but the decrease in water vapor flux may offset the positive contribution of convergence. As a result, the summer precipitation exhibited a weak declining trend from 1984 to 2014.



a difference between the eastern and the western areas of the catchment [7]. The abovementioned reasons may contribute to the spatial variability of precipitation in HRB.

The EOF analysis demonstrates that the first EOF displayed the main features of the temporal variability in the whole basin. The increasing trend of precipitation from 1984 to 2014 may be mainly derived from changes in large-scale weather systems, which were mainly influenced by atmospheric circulation [26–28]. For most stations, a slight but noticeable increasing trend was also detected in precipitation at an annual scale. It was reported that the water vapor over the northwest region exhibited an increasing trend since the late 1980s [27,29], and the high-altitude wind field in Northwest China has been favorable for the transmission of water vapor from south to north in recent years [26,27]. Weakened by the Ural Mountains ridge and the East Asian trough, the westerly wind is weaker and the south wind is stronger in Northwest China [10,30,31]. Such circulation is favorable for the northward transmission of southern moisture from the Indian Ocean and the Western Pacific [27,32]. This may be the main cause of the increase in precipitation in the HRB. The second EOF displayed approximately symmetric characteristics of precipitation between the northeast and the southwest region, and it can be inferred that the opposite tendency became more and more obvious from 1984 to 2014. The main reason for this may be the impact of small- and medium-scale weather systems [14,33,34]. However, when compared with a large-scale weather system, the effect on precipitation was less significant. Previous studies also found that precipitation in the western region to the northwest of the HRB increased significantly under global warming and accelerating water circulation [7,33]. In addition, Shi et al. [6,35] found that the climate was basically characterized by the development of warm and wet weather from the end of the Little Ice Age until the 1980s, especially in Northwest China. However, the cause of the second EOF has yet to be determined.

Qu et al. [36] reported that as a response to climate warming status after 1998, there was a decreasing trend in the number of extreme high-temperature events in Northwest China during the last 20 years. In the HRB, there was weakened climate warming, which is like the hiatus, from the late 1990s to the early 2010s [16]. Here, our findings suggest that precipitation changes in HRB also responded to the climate warming hiatus. There was a rise in precipitation, especially in the autumn, in the HRB around 1997, which approximately corresponded to the beginning of the hiatus.

The changes in atmospheric circulation and physical structures, such as temperature, vertical upward motion, vapor transmission, and its convergence from 1984 to 2014 were all favorable for autumn precipitation. First, from 1984–1997 to 1998–2014, the changes in circulation at a pressure level of 500 hPa were characterized by a wind direction shift from westerly to easterly in the summer and by a wind direction shift from northerly to southerly in the autumn. Under these circumstances, the southward-moving cold air is favorable for the activities of a low-pressure system such as plateau vortex and shear line, and may lead to more precipitation in the HRB in autumn [30,32]. With the transformation of general circulation of 500 hPa from divergence to convergence in the autumn, the increase in atmospheric instability and the transmission of water vapor were also strengthened. Second, the vertical upward motion provided good dynamic conditions for precipitation in the autumn. The strong upward movement is also beneficial to the development of low-pressure disturbances in the plateau region [31,37]. Finally, stronger water vapor transmission and its convergence provide the necessary water vapor conditions for precipitation in autumn. Zhang and Xu [38] reported that water vapor for precipitation in spring and summer mainly came from the ocean air mass; conversely, precipitation in autumn and winter was mostly derived from continental recycled water in the HRB. Previous studies also found that the proportion of precipitation formed by continental recycling and water evaporation increased significantly in the HRB [38–41]. All these factors may together contribute to the increase in autumn precipitation in the HRB.

## 5. Conclusions

The ground measurements of precipitation from 25 stations across the southern part of HRB from 1984 to 2014 were analyzed with statistical methods. The findings demonstrate that the regional

annual precipitation and NDP increased by 13.1 mm and 3.2 days per decade, respectively, from 1984 to 2014. Such increases were mainly due to the increase in autumn precipitation, the slope of which was 13.7 mm per decade. There was an abrupt increase around 1997. This point corresponded to the climate warming hiatus. The findings suggest that the increase in autumn precipitation was induced by atmospheric circulation, which may lead to more water vapor flux, intensified upward motion, and the convergence of dynamic conditions. This study suggests that, along with the climate warming hiatus, the large-scale circulation changed and, hence, the regional/local precipitation changed as a response.

**Acknowledgments:** This research was supported by the National Key R&D Program of China on Global Change (Grant nos. 2016YFA0600401, 2017YFA0603301), the National Natural Science Foundation of China (Grant nos. 41471171, 91425304), the Youth Innovation Promotion Association CAS (Grant no. 2015038), and Kezhen Outstanding Young Scholars from IGSNRR (Grant no. 2015RC101).

**Author Contributions:** Xuezhen Zhang conceived and designed the experiments; Pei Li and Deshuai Li analyzed the data; Xuezhen Zhang and Pei Li wrote the paper.

**Conflicts of Interest:** The authors declare no conflict of interest.

## References

- Allen, M.R.; Ingram, W.J. Constraints on future changes in climate and the hydrologic cycle. *Nature* **2002**, *418*, 224–232. [[CrossRef](#)] [[PubMed](#)]
- Cao, L.; Dou, Y.X.; Zhang, D.Y. Effect of climate change on ecological environment of Heihe Field. *Arid Meteorol.* **2003**, *21*, 45–49.
- Shi, Y.F.; Shen, Y.P.; Li, D.L.; Zhang, G.W.; Ding, Y.J.; Hu, R.J.; Kang, E. Discussion on the present climate change from warm2dry to warm2wet in northwest China. *Quat. Sci.* **2003**, *23*, 152–164.
- Ding, Y.J.; Ye, B.S.; Zhou, W.J. Temporal and spatial precipitation distribution in the Heihe Catchment, Northwest, during the past 40 a. *J. Glaciol. Geocryol.* **1999**, *21*, 42–48.
- Fu, Y.Z.; Cao, L. The area rainfall analysis and climatic feature of Heihe River drainage. *Gansu Meteorol.* **2002**, *20*, 8–10.
- Zang, C.; Liu, J. Trend analysis for the flows of green and blue water in the Heihe River basin, northwestern China. *J. Hydrol.* **2013**, *502*, 27–36. [[CrossRef](#)]
- Wang, K.L.; Cheng, G.D.; Jiang, H. Atmospheric hydrologic cycle over the Qilian-Heihe River Valley. *Adv. Water Sci.* **2003**, *14*, 91–97.
- Li, H.Y.; Wang, K.L.; Jiang, H.; Yu, T. Study of the Precipitation in the Heihe River Basin: Progress and Prospect. *J. Glaciol. Geocryol.* **2009**, *31*, 334–341.
- Wang, F.; Niu, J. The Implication of Climate Signal for Precipitation in the Heihe River Basin, Northwest China. *Adv. Meteorol.* **2016**, *4*, 1–9. [[CrossRef](#)]
- Liu, H.L.; Zhang, Q.; Guo, J.Q. Spatial differentiation of spring precipitation in the Heihe River Basin and its correlation with the river flow. *J. Desert Res.* **2014**, *34*, 1633–1640.
- Ding, R.; Wang, F.C.; Wang, J.; Liang, J.N. Analysis on Spatial-temporal Characteristics of Precipitation in Heihe River Basin and Forecast Evaluation in Recent 47 Years. *J. Desert Res.* **2009**, *29*, 335–341.
- Zhao, H.Y.; Jiang, H.; Wang, K.L.; Yu, Y.X.; Yang, Y.F. The Atmospheric Water Resource over the Qilian-Heihe Valley. *Acta Meteorol. Sin.* **2005**, *20*, 90–97.
- Medhaug, I.; Stolpe, M.; Fischer, E.; Knutti, R. Reconciling controversies about the ‘global warming hiatus’. *Nature* **2017**, *545*, 41–47. [[CrossRef](#)] [[PubMed](#)]
- Schiermeier, Q. IPCC: Despite Hiatus, Climate Change Here to Stay. 2013. Available online: <https://www.nature.com/news/ipcc-despite-hiatus-climate-change-here-to-stay-1.13832> (accessed on 27 September 2013).
- Kosaka, Y.; Xie, S.P. Recent global-warming hiatus tied to equatorial Pacific surface cooling. *Nature* **2013**, *501*, 403–407. [[CrossRef](#)] [[PubMed](#)]
- Zhao, Y.; Zhang, B.; Zhang, Y. Impact of climate change on agriculture production in the Heihe River Basin in recent 50 years. *J. Arid Land Res. Environ.* **2012**, *26*, 130–136.
- Gerard, B.; Eduardo, Z.; Hans, V.S. Estimation of Precipitation by Kriging in the EOF Space of the Sea Level Pressure Field. *J. Clim.* **1997**, *12*, 1078–1085.

18. Mann, H.B. *Nonparametric Tests against Trend*; Econometric Society: Cleveland, OH, USA, 1945; Volume 13, pp. 245–259.
19. Bradley, J.V. *Distribution-Free Statistical Tests*; Prentice-Hall: Englewood Cliffs, NJ, USA, 1968.
20. Kendall, M. *Rank Correlation Measures*; Charles Griffin: London, UK, 1975; p. 202.
21. Pan, X.; Li, X.; Yang, K.; He, J.; Zhang, Y.; Han, X. Comparison of downscaled precipitation data over a mountainous watershed: A case study in the Heihe River basin. *J. Hydrometeorol.* **2014**, *15*, 1560–1574. [[CrossRef](#)]
22. Zhang, X.; Xiong, Z.; Zheng, J.; Ge, Q. High-resolution precipitation data derived from dynamical downscaling using the WRF model for the Heihe River Basin, Northwest China. *Theor. Appl. Climatol.* **2018**, *131*, 1249–1259. [[CrossRef](#)]
23. Zhang, L.; Wang, S.G.; Shang, K.Z.; Yang, D.B. Research on vapor and precipitation resources over the Qilian Mountain area. *Arid Meteorol.* **2007**, *25*, 14–20.
24. Wang, J.Y.; Wang, Y.H.; Wang, S.L.; Yu, P.T.; Zhang, X.L.; Ge, S.L. A preliminary study on the precipitation variation of complex watershed on forestry and grasses of Qilian Mountain. *Res. For.* **2006**, *19*, 416–422.
25. Gao, Y.H.; Cheng, G.D. Several points on mass and energy interaction between land surface and atmosphere in the Heihe River Basin. *Adv. Earth Sci.* **2008**, *23*, 779–784.
26. Sun, Y.; Ding, Y.H. Role of summer monsoon in anomalous precipitation patterns during 1997 flooding season. *J. Appl. Meteorol. Sci.* **2002**, *13*, 277–287.
27. Yu, Y.X.; Wang, J.S.; Li, Q.Y. Spatial and Temporal Distribution of Water Vapor and Its Variation Trend in Atmosphere over Northwest China. *J. Glaciol. Geocryol.* **2003**, *25*, 149–156.
28. Jin, L.Y.; Fu, J.L.; Chen, F.H. Spatial and temporal distribution of water vapor and its relationship with precipitation over Northwest China. *J. Lanzhou Univ. Nat. Sci.* **2006**, *42*, 1–6.
29. Liu, H.L.; Li, D.L.; Guo, J.Y. Abnormal Space Distribution of Precipitation in Hexi Corridor in the Late Spring and Early Summer and Its Inter-Decadal Variability. *J. Glaciol. Geocryol.* **2004**, *26*, 55–60.
30. Tao, J.H.; Wu, H.B.; Zhang, T.J. Study on the relationship between the climate change in northwest China and the abnormality of earcultation. *Arid Zone Res.* **2006**, *23*, 632–636.
31. Wang, K.L.; Jiang, H.; Zhao, H.Y. Atmospheric water vapor transport from westerly and monsoon over the North West China. *Adv. Water Sci.* **2005**, *16*, 432–438.
32. Zhu, Y.F.; Yu, R.C. Interannual variation of summer precipitation in the west of Sichuan Basin and its relationship with large-scale circulation. *Chin. J. Atmos. Sci.* **2003**, *27*, 1045–1056.
33. Cao, L.; Dou, Y.X. The spatial and temporal characteristics and forecasting method of precipitation in Heihe Field. *Arid Meteorol.* **2005**, *23*, 35–39.
34. Wang, B.L.; Dong, A.X.; Wang, L. EOF analysis of summer precipitation in Northwest China and the relation between it and 500 hPa height field. *Plateau Meteorol.* **1995**, *14*, 342–347.
35. Shi, Y.F.; Shen, Y.P. Signal, Impact and Outlook of Climatic Shift from Warm—Dry to Warm Humid in Northwest China. *Sci. Technol. Rev.* **2003**, *2*, 54–57.
36. Qu, S.L.; Tong, J.L.; Tang, R.; Li, J.Y. Changes in the extremely high temperature in Northwest China and its response to the stagnation of global warming. *J. Meteorol. Environ.* **2017**, *33*, 78–85.
37. Chen, Q.L.; Liu, X.R.; Fan, G.Z.; Hua, W. Features of summer precipitation change over the west Sichuan plateau and its relationship with large-scale circulations. *J. Desert Res.* **2010**, *30*, 706–711.
38. Zhang, Y.H.; Xu, Y.Q. Precipitation from different water vapor sources in the Heihe River basin, China. *Arid Land Geogr.* **2008**, *31*, 403–408.
39. Lan, Y.C.; Ding, Y.J.; Liu, J.Q.; Yu, T. Change of water resources in mountainous area of Heihe River under global-warming scene. *J. Desert Res.* **2005**, *25*, 863–868.
40. Chen, Y.M.; Cao, J.; Wang, C.H. Precipitation variation over southeastern China in winter and its circulation pattern. *Trans. Atmos. Sci.* **2013**, *36*, 323–330.
41. Zhang, J.; Li, D.L. Analysis on distribution character of rainfall over Qilian Mountain and Heihe valley. *Plateau Meteorol.* **2004**, *23*, 81–88.

